Melt equilibration depths as sensors of lithospheric thickness during Eurasia-Arabia collision and the uplift of the Anatolian Plateau

M. R. Reid[1], J.R. Delph[2], M.A. Cosca[3], W.K. Schleiffarth[1], and G. Gençalioğlu Kuşcu[4]
[1]*Geoscience Division, School of Earth and Sustainability, Northern Arizona University, Flagstaff, AZ 86011*
[2]*Department of Earth, Environmental and Planetary Sciences, Rice University, Houston, Texas, USA*
[3]*U.S. Geological Survey, Denver Federal Center, Denver, Colorado, USA*
[4]*Department of Geological Engineering, Muğla Sıtkı Koçman University, Kötekli, Muğla, Turkey*

Supplementary Material

The Lithosphere-Asthenosphere Boundary

The lithosphere-asthenosphere boundary (LAB) represents the rheological change from rigid (thermally conductive) to ductile (convective) material in the Earth's upper mantle (Sleep, 2005). Despite the implications of its name, the LAB generally represents a diffuse change in seismic properties, making it rather challenging to image (Fischer et al., 2010). However, measuring seismic waves sensitive to temperature variations and fluids (e.g., shear waves) alongside measurements sensitive to vertical changes in velocity structure (e.g., receiver functions), can highlight the likely location of the LAB when interpreted in light of global models of seismic velocities and the petrophysical characteristics of typical upper mantle material.

The Shear Wave Velocity of Mantle Lithosphere

Based on global compilations of major seismic phase travel times for earthquakes as a function of distance, the average shear wave velocity of the uppermost mantle of the Earth is ~4.5 km/s (4.49 km/s, PREM: Dziewonski and Anderson, 1981; 4.47 km/s, IASP91: Kennett and Engdahl, 1991; 4.48 km/s, AK135: Kennett et al., 1995). As most of Earth's crust is underlain by lithospheric mantle, we can infer that these are the typical velocities for mantle lithosphere. It is generally accepted that the upper mantle primarily comprises peridotite, and thus these velocities likely correspond to in-situ velocity averages of peridotite in the upper mantle.

We can also calculate the velocities for mantle peridotite by creating theoretical solids based on stable mineral assemblages and their elastic properties at a given temperature and pressure. In **Fig. DR1**, we show the estimated velocity for a Hashin-Shtrikman solid of peridotite composition (Abers and Hacker, 2016). These velocities are generally higher than what we would expect given global averages of shear wave velocity in the upper mantle (>4.5 km/s). Using other theoretical velocity relationships for solids (such as Voight-Reuss-Hill) return similar results.

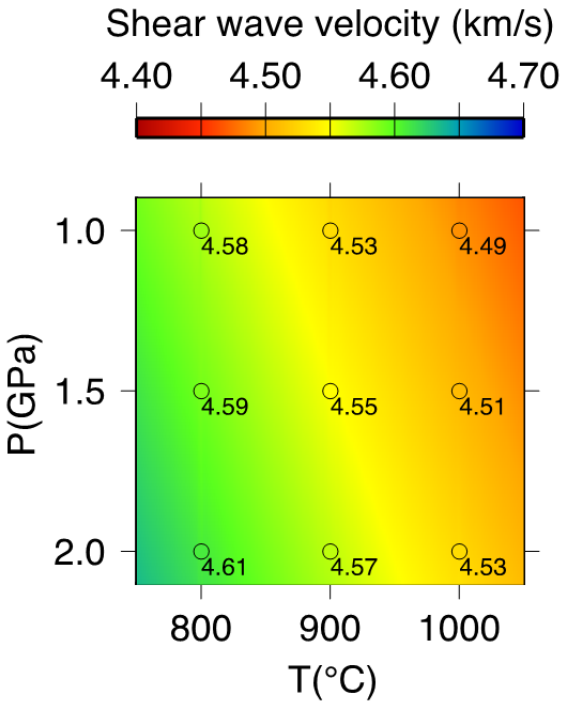

Figure DR1: Estimated shear wave velocities for a Hashin-Shtrikman solid of peridotite (harzburgite, in this case) composition. Colored circles represent suit of P-T conditions used for calculation. Background color from interpolation of these results. Using a lherzolite composition results in negligibly different velocities (~0.01 km/s).

The Creation of the Shear Wave Velocity Model

The creation of this velocity model is described in detail in Delph, Abgarmi, et al. (2017), with the methodology outlined by Delph et al. (2015) and Delph, Ward, et al. (2017). The interested reader is referred to those manuscripts for the technical details of the methodology and velocity model creation, which will only be briefly outlined here.

We combined the P-wave receiver function analyses of Abgarmi et al. (2017) with ambient noise- and earthquake-derived Rayleigh wave phase velocity measurements from a recently deployed temporary seismic network distributed throughout central Anatolia (CD-CAT Array; Abgarmi et al., 2017) to create a 3D shear wave velocity model for central Anatolia down to 150 km depth. For the ambient noise analysis, we used data from 282 seismic stations over a period of 10 years distributed throughout the Anatolian plate from Greece to easternmost Anatolia. We obtained reliable results for Rayleigh wave phase velocities between 8-50 seconds, which is sensitive to the shear-wave velocity structure to ~80 km depth. We combined these measurements with measurements from earthquake-generated Rayleigh waves recorded at the CD-CAT stations, obtaining reliable phase velocity measurements from 40-111 seconds using two-plane wave tomography (Forsyth and Li, 2005). This period range is sensitive to the shear wave velocity structure from ~40-150 km depth. Both the ambient noise and two-plane wave tomographic inversions used lateral smoothing parameters of 50 km, which in practicality, means that any seismic anomaly greater than 50 km will be well-resolved in space and amplitude, while

smaller anomalies may be well resolved in space, but will have diminished amplitudes due to smoothing.

In order to mitigate for the very broad vertical sensitivities of Rayleigh waves to shear wave velocity structure and relative inability to constrain depths to boundaries (e.g., Lebedev et al., 2013), we combine the surface wave dispersion data with the P-wave receiver function data of Abgarmi et al. (2017) in a joint mathematical inversion following the methodology described by Julià et al. (2000). These datasets have complementary sensitivities, as receiver functions are very sensitive to depths to velocity discontinuities. The receiver function are computed to focus on 1Hz seismic energy, corresponding to a theoretical vertical resolution of ~1 km. The joint inversion of these datasets results in the creation of a velocity model that is relatively independent of starting velocity model, and thus all structure in the final model is fundamentally driven by the data, as opposed surface wave inversion techniques that only use dispersion information (e.g., full-waveform inversions). A damping term in the joint inversion meant to promote solution stability has the effect of limiting the magnitude of the change in velocity across a boundary, effectively acting to smooth out velocity jumps in the model. This results in a decrease in the vertical resolution of the final shear wave velocity model when compared to the receiver function frequency content to ~1-5 km in the crust and upper mantle. This resolution is still much higher than dispersion only inversions, whose vertical resolution is generally on the order or 20-50 km in the crust and uppermost mantle.

Maximum Gradient Algorithm for Estimating LAB Depths

This algorithm and its results are described in Delph, Abgarmi, et al. (2017) A brief overview is given below:

Given the seismic velocity and petrophysical estimates for lithospheric mantle peridotite having velocities greater than or ~4.5 km/s, we develop a proxy that determine the spatial extend of the mantle lithosphere. Due to the uncertainties in vertical and lateral resolution mentioned above, we chose a more conservative value to represent mantle lithosphere (4.4 km/s). To estimate the depth to the LAB consistently across the study area, we wrote an algorithm that obtains the depth to the maximum negative velocity gradient after a velocity of 4.4 km/s is reached. This is a relatively common way to try to map out LAB depths given a shear wave velocity model (Eaton et al., 2009; Fischer et al., 2010). When applied to our 3D velocity model, this returns LAB depth estimates for each grid point, which is used to create the surface indicated by the red lines in Fig. 2C (also see Delph, Abgarmi, et al. 2017 for more examples and a regional map of LAB depth estimates). Fig. DR2 (below) visually shows how this algorithm works.

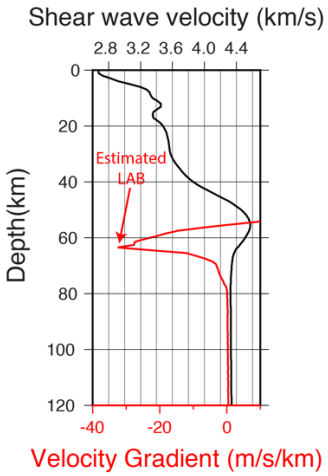

Figure DR2: A vertical profile from the shear wave velocity model for central Anatolia (black) and its derivative (red). We take the largest negative value to represent the depth to the LAB after a velocity of 4.4 km/s is reached. We assume 4.4 km/s represents typical mantle lithosphere (a rather conservative estimate given that the expected Vs of mantle lithosphere should be ~4.5 km/s). The solution here is at 63 km depth. See Delph et al. 2017 for further discussion on the algorithm.

Supplementary Tables

2019335_Table DR1.xlsx

2019335_Table DR2.xlsx

References

Abers, G.A., and Hacker, B.R., 2016, A MATLAB toolbox and Excel workbook for calculating the densities, seismic wave speeds, and major element composition of minerals and rocks at pressure and temperature: Geochemistry, Geophysics, Geosystems, v. 17, p. 616–624, doi: 10.1002/2015GC006171.

Abgarmi, B., Delph, J.R., Ozacar, A.A., Beck, S.L., Zandt, G., Sandvol, E., Turkelli, N., and Biryol, C.B., 2017, Structure of the crust and African slab beneath the central Anatolian plateau from receiver functions: New insights on isostatic compensation and slab dynamics: Geosphere, p. 1–14, doi: 10.1130/GES01509.1.

Delph, J.R., Abgarmi, B., Ward, K.M., Beck, S.L., Özacar, A.A., Zandt, G., Sandvol, E., Türkelli, N., and Kalafat, D., 2017, The effects of subduction termination on the continental lithosphere: Linking volcanism, deformation, surface uplift, and slab tearing in central Anatolia: Geosphere, v. 13, p. 1788–1805, doi: 10.1130/GES01478.1.

Delph, J.R., Ward, K.M., Zandt, G., Ducea, M.N., and Beck, S.L., 2017, Imaging a magma plumbing system from MASH zone to magma reservoir: Earth and Planetary Science Letters, v. 457, p. 313–324, doi: 10.1016/j.epsl.2016.10.008.

Delph, J.R., Zandt, G., and Beck, S.L., 2015, A new approach to obtaining a 3D shear wave velocity model of the crust and upper mantle: An application to eastern Turkey: Tectonophysics, v. 665, p. 92–100, doi: 10.1016/j.tecto.2015.09.031.

Dziewonski, A.M., and Anderson, D.L., 1981, Preliminary reference Earth model: Physics of the

Earth and Planetary Interiors, v. 25, p. 297–356, doi: 10.1016/0031-9201(81)90046-7.
Eaton, D.W., Darbyshire, F., Evans, R.L., Grütter, H., Jones, A.G., and Yuan, X., 2009, The elusive lithosphere-asthenosphere boundary (LAB) beneath cratons: Lithos, v. 109, p. 1–22, doi: 10.1016/j.lithos.2008.05.009.
Fischer, K.M., Ford, H.A., Abt, D.L., and Rychert, C.A., 2010, The Lithosphere-Asthenosphere Boundary: Annual Review of Earth and Planetary Sciences, v. 38, p. 551–575, doi: 10.1146/annurev-earth-040809-152438.
Forsyth, D.W., and Li, A., 2005, Array analysis of two-dimensional variations in surface wave phase velocity and azimuthal anisotropy in the presence of multipathing interference, *in* Seismic Earth: Array Analysis of Broadband Seismograms, p. 81–97, doi: 10.1029/157GM06.
Julià, J., Ammon, C.J., Herrmann, R.B., and Correig, A.M., 2000, Joint inversion of receiver function and surface wave dispersion observations: Geophysical Journal International, v. 143, p. 99–112, doi: 10.1046/j.1365-246x.2000.00217.x.
Kennett, B.L.N., and Engdahl, E.R., 1991, Traveltimes for global earthquake location and phase identification: Geophysical Journal International, v. 105, p. 429–465, doi: 10.1111/j.1365-246X.1991.tb06724.x.
Kennett, B.L.N., Engdahl, E.R., and Buland, R., 1995, Constraints on seismic velocities in the Earth from traveltimes: Geophysical Journal International, v. 122, p. 108–124, doi: 10.1111/j.1365-246X.1995.tb03540.x.
Lebedev, S., Adam, J.M.C., and Meier, T., 2013, Mapping the Moho with seismic surface waves: A review, resolution analysis, and recommended inversion strategies: Tectonophysics, v. 609, p. 377–394, doi: 10.1016/j.tecto.2012.12.030.
Sleep, N.H., 2005, EVOLUTION OF THE CONTINENTAL LITHOSPHERE: Annual Review of Earth and Planetary Sciences, v. 33, p. 369–393, doi: 10.1146/annurev.earth.33.092203.122643.